Available online at www.sciencedirect.com
SCIENCE DIRECT®
Journal of the European Ceramic Society 25 (2005) 1675–1680
www.elsevier.com/locate/jeurceramsoc

# $Bi_2O_3$ vaporization from ZnO-based varistors

M. Peiteado*, M.A. de la Rubia, M.J. Velasco, F.J. Valle, A.C. Caballero

*Instituto de Cerámica y Vidrio, Consejo Superior de Investigaciones Científicas, 28049 Madrid, Spain*

Received 4 March 2004; received in revised form 1 June 2004; accepted 20 June 2004
Available online 13 August 2004

**Abstract**

$Bi_2O_3$-doped ZnO ceramic varistors are usually sintered at temperatures near to 1200 °C in the presence of a Bi-rich liquid phase, which is partially vaporized during the sintering process. Volatilization of bismuth oxide depends on the total surface area in direct contact to the reaction atmosphere and this in turn is related to the area/volume ratio of the ceramic compact. This loss of $Bi_2O_3$ has a significant role on the development of the varistor microstructure and more specifically ZnO grain growth, which is strongly enhanced by the presence of the liquid phase, should be particularly affected. In the present paper, X-ray fluorescence analysis is performed to describe the $Bi_2O_3$ vaporization profile as a function of distance to the outer surface, taking into account its influence on microstructural evolution.


*Keywords:* Sintering; Vaporization; Grain size; Varistors; ZnO; $Bi_2O_3$

## 1. Introduction

Zinc oxide-based varistors are multiphase ceramic devices which exhibit highly non-linear current–voltage characteristics.[1–3] This extensive non-ohmic characteristic together with an ability to repeatedly withstand relatively high power pulses has resulted in the widespread application of varistors as voltage surge protectors in electrical circuits.[4,5] The device non-linearity depends on density and chemical composition of the material, and moreover on the microstructure development.[6,7] Although several metal oxides are used as additives, the most widely used system for ceramic varistor manufacturing is based in the ternary ZnO–$Bi_2O_3$–$Sb_2O_3$, where $Bi_2O_3$ plays an essential role to impart non-linear behaviour to the material.[3,8,9]

The ZnO–$Bi_2O_3$ binary system has a eutectic at 750 °C[10] which gives rise to liquid formation and hence densification. Grain growth kinetics will be determined by the specific diffusion mechanisms of liquid phase sintering.[11–13] With the addition of $Sb_2O_3$, the system is further complicated as the three oxides react at low temperatures to form a pyrochlore type phase which decomposes above 900 °C to a zinc–antimony spinel type phase and liquid $Bi_2O_3$.[6,14,15] This $Bi_2O_3$-rich phase wets the grain boundaries forming intergranular layers that recede during cooling to the pockets created by grain packing. The presence of a very thin Bi-rich amorphous film (1–2 nm) or intergranular segregation of Bi atoms at the ZnO/ZnO grain boundaries, contributes to the formation of potential barriers to electrical conduction in the vicinity of the ZnO interfaces.[16–19]

Since Matsuoka's first work in the earlier 1970s,[1] a number of efforts have been carried out in an attempt to more fully understand the influence of bismuth and other minor components on the microstructure and electrical properties of ZnO-based varistors. However, the exact role of each is often hard to assess with commercially available ceramics consisting of up to 10 different oxides such as ZnO, $Bi_2O_3$, $Sb_2O_3$, $Co_3O_4$, $SnO_2$, $Cr_2O_3$, MnO, etc. Furthermore, many sources of problems may arise from the ceramic processing due to the number of industrial operations that need specific care: quality control of raw materials, slip homogeneity, pressing operations, sintering, etc. Among these operations, the composition after sintering is difficult to handle because several oxides with high vapour pressure are used in typical ZnO varistor formulation.[20] That means that the

* Corresponding author.
*E-mail address:* peitead@icv.csic.es (M. Peiteado).

0955-2219/$ – see front matter © 2004 Elsevier Ltd. All rights reserved.
doi:10.1016/j.jeurceramsoc.2004.06.006

composition is likely to change after sintering because of component vaporization. In particular weight loss by uncontrolled $Bi_2O_3$ vaporization becomes a crucial parameter for varistor manufacturing.[21–23]

Several efforts have been carried out to describe the influence of different $Bi_2O_3$ contents on microstructure and electrical properties of varistor devices. In most cases the authors pointed out that bismuth oxide is lost at high temperature but without quantifying it.[16,21,24,25] Few are concerned with this quantification of $Bi_2O_3$ vaporization during the sintering process. Chiang et al.[26] have reported a loss of 19 wt.% of bismuth oxide when sintering at 1150 °C for 90 min by emission spectroscopy. They also found cobalt oxide vaporization when using this technique. More recently Metz et al.[22] have tried to quantify $Bi_2O_3$ vaporization by using thermogravimetry to follow the loss of weigh observed during the sintering process. They used pyrochlore and spinel phases previously synthesized as raw materials, with antimony oxide already in the oxidation state V, so avoiding the weight profit due to $Sb_2O_3$ oxidation that could mask weight loss measurements. Nevertheless, they reported results that show $Bi_2O_3$ losses up to 95 wt.% depending on the temperature and soaking time. To some extent such loss of material needs to be controlled, but even more it appears to be necessary to determine the profile of losses within the ceramic compact, since it is expected not to be homogeneous. Vaporization of volatile components depends on the total surface area exposed to the reaction atmosphere, hence $Bi_2O_3$ loss should be different as distance to the surface changes. Furthermore, this has to be related to the area/volume ratio ($A/V$) of the green compact which determines the total surface area exposed to the environment.[27] This is the focus of the present paper, in which we use X-ray fluorescence (XRF) to quantify $Bi_2O_3$ vaporization and to establish the $Bi_2O_3$ losses as a function of distance to the surface. The results are particularly relevant for manufacturing commercial varistors. The influence of this non-homogeneous $Bi_2O_3$ vaporization on the microstructure development is also discussed in terms of ZnO grain growth.

## 2. Experimental procedure

### 2.1. Sample preparation

Bismuth oxide vaporization in typical ceramic varistors was studied by preparing samples from the following reference composition: ZnO (95.32 mol%), $Bi_2O_3$ (0.47%), $Sb_2O_3$ (1.71%), $Co_3O_4$ (0.47%), NiO (1.28%) and MnO (0.75%). Dense materials were obtained using a classical mixed-oxide route; suitable amounts of the chemically pure commercial oxides were homogenized in a planetary mill for 2 h in ethanol, then dried at 60 °C and sieved through a 100 μm mesh. Two samples of 250 g weight, labelled A1 and A2, were uniaxially pressed at 80 MPa into cylinders of 3.5 cm height × 5.4 cm diameter ($A/V$ equal to 1.3 $cm^{-1}$) quite similar to commercial dimensions for high voltage applications. Sintering conditions were chosen so that a considerable vaporization of $Bi_2O_3$ should be observed: 1240 °C for 4 h in air. The green compacts were placed on a cordierite sheet covered with previously sintered varistor powder in order to avoid material diffusion into the substrate. For XRF analysis sample A1 was transversally cut into seven discs from the upper face directly exposed to the air (upper slice) to the bottom face in contact with the cordierite sheet (floor slice). Six longitudinal cuts were obtained from sample A2, from the external surface to the centre of the sintered ceramic.

In order to study the influence of $A/V$ ratio on $Bi_2O_3$ vaporization, one more sample of 8 g weight and 1.37 cm height × 1.5 cm diameter ($A/V$ equal to 4.1 $cm^{-1}$), sample A3, was sintered at the same temperature and time and cut transversally into seven slices (no longitudinal XRF measurable cuts were possible with such dimensions). Additionally one sample without bismuth oxide was also sintered at 1240 °C/4 h, as a reference to check if any other element interfered with the BiL$\alpha_1$ line when analyzing XRF spectra (sample A4).

### 2.2. Characterization methods

XRF analyses were carried out using a Spectrometer (Model MagiX PW 2424, Philips, Eindhoven, Netherlands) with rhodium X-ray tube, 2.4 kW generator and five-position crystal charger. The spectrometer is also equipped with the $IQ^+$ analytical software for qualitative and semi-quantitative analysis, which includes fundamental parameters for inter-elemental correction calculations. The operating conditions were LIF200 and PE analyzing crystals, no primary beam filter, 150 μm sample collimator, vacuum atmosphere and flow-proportional and scintillation detector. Measures of the intensity of the L$\alpha_1$ radiation of Bi were performed in each of the slices over a circular flat surface of 27 mm which corresponds to the measurement area of the spectrometer sample holder, and averaging up to five samplings per face. This area is fixed for all measurements to apply the $IQ^+$ analysis method. As the mass absorption coefficient $\mu_m$ of the whole sample is strongly influenced by the mass coefficient of the majority component, zinc oxide, $\mu_{ZnO}$, the penetration thickness will be roughly the same for all the analyzed slices.

For microstructural observations scanning electron microscopy (SEM) of polished and chemically etched surfaces was carried out using a Cold Field Emission-Scanning Electron Microscope (Model S-4700, Hitachi, Tokyo, Japan). ZnO grain size was evaluated from SEM micrographs by an image processing and analysis program that measures the surface of each ZnO grain and transforms its irregularly shaped area into a circle of equivalent diameter. More than 800 grains were considered for each measurement.

## 3. Results

The varistor theoretical composition as well as the chemical compositions before and after sintering are summarized in

Table 1
Varistor chemical composition before and after sintering in wt.% (normalized results to 100%)

| Component | Formulated composition | Composition before sintering[a] | Composition after sintering at 1240 °C/4 h[a] |
|---|---|---|---|
| MnO | 0.60 | 0.62 | 0.60 |
| $Co_3O_4$ | 1.33 | 1.25 | 1.19 |
| NiO | 1.14 | 1.18 | 1.17 |
| ZnO | 88.7 | 88.7 | 89.4 |
| $Sb_2O_3$ | 5.69 | 5.7 | 5.70 |
| $Bi_2O_3$ | 2.54 | 2.55 | 1.95 |

[a] Obtained with $IQ^+$ analysis from XRF measurements.

Table 1. These data correspond to the upper transverse slice of sample A1 with an *A*/*V* ratio similar to industrial dimensions. Although the $IQ^+$ system allows only semi-quantitative analysis, considerable agreement between the expected formulated values and the experimental ones obtained from XRF measurements can be inferred from this Table 1. Only the $Co_3O_4$ and $Bi_2O_3$ contents differ from the formulated composition. Both may be attributed to component volatilization during the firing process. As previously mentioned, $Co_3O_4$ vaporization was observed to occur at high temperatures by Chiang et al.[26] It is primarily added to the varistor composition to enhance the device non-linearity. For the purpose of this paper, we have centred our research on the other vaporized component, the $Bi_2O_3$, which is the varistor forming dopant to the ZnO.

$IQ^+$ analysis was extended to the totality of the non-coincident faces in the transverse and longitudinal sections of samples A1 and A2, together with measures of $BiL\alpha_1$ radiation intensity (Kcps). It should be noted that these readings correspond to the integrated concentration of the whole measured area. Table 2 displays the results of $Bi_2O_3$ XRF analysis for sample A1, from the upper face to the bottom floor just placed over the cordierite sheet with varistor sintered powder. Data in Table 2 shows differences in the $Bi_2O_3$ concentration when calculated from the intensity measurements (Kcps) with respect to that obtained with $IQ^+$ and assuming a linear response. These differences are due to the semi-quantitative character of $IQ^+$ so in fact this analysis system is mainly used as a guide line to corroborate the calculated values. In these terms, the $Bi_2O_3$ vaporization percentage is obtained from the $Bi_2O_3$ concentration data calculated from the $BiL\alpha_1$ radiation intensity. Location of the seven transversal disks of sample A1 and graphic representation of $Bi_2O_3$ vaporization as a function of distance to the surface is depicted in Fig. 1. The same analysis was performed for sample A2 and its six longitudinal slices; results are displayed in Table 3 and depicted in Fig. 2.

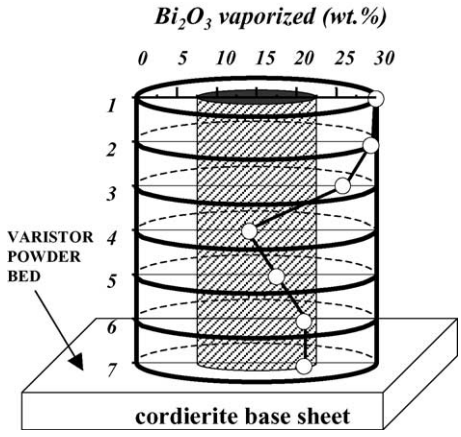


Fig. 1. Transversal gradient of $Bi_2O_3$ vaporization (in wt.%) for sample A1, from the upper slice (labeled 1) to the floor face (labeled 7). *A*/*V* ratio = 1.3 $cm^{-1}$. Shaded zone corresponds to the XRF analyzed area (Ø = 27 mm).

In case of sample A3, it was noted that its smaller dimensions do not allow longitudinal cuts and only seven transversal slices were obtained to follow $Bi_2O_3$ vaporization. Besides, the $IQ^+$ semi-quantitative analysis requires specimens with a 27 mm minimum diameter. It was not the case of A3 slices, so that analysis in this sample has been limited to $BiL\alpha_1$ line intensity measurements. To hold the pellets on the XRF sample holder, a circular mask made of teflon was manufactured with 0.2 mm in thickness and 10 mm in diameter for X-ray radiation entry. Results of $Bi_2O_3$ vaporization for sample A3 are displayed in Table 4 and graphically depicted in Fig. 3.

Table 2
Transversal profile of $Bi_2O_3$ vaporization in sample A1[a]

| | XRF intensity (Kcps) | $[Bi_2O_3]$ from $IQ^+$ (wt.%)[b] | Calculated $[Bi_2O_3]$ (wt.%) | % $Bi_2O_3$ vaporized |
|---|---|---|---|---|
| Upper slice | 33044 | 1.82 | 1.78 | 29.7 |
| Slice 2 | 33156 | 1.84 | 1.79 | 29.5 |
| Slice 3 | 34719 | 1.98 | 1.88 | 26.1 |
| Slice 4 | 40533 | 2.16 | 2.19 | 13.8 |
| Slice 5 | 38814 | 2.20 | 2.09 | 17.4 |
| Slice 6 | 37811 | 1.88 | 2.04 | 19.6 |
| Floor slice | 37098 | 2.06 | 2.00 | 21.1 |
| Green compact | 47008 | 2.55 | 2.54[c] | |

[a] *A*/*V* = 1.3 $cm^{-1}$.
[b] RSD ± 0.30, corresponding to $\sigma < 0.01\%$.
[c] Formulated composition.

Table 3
Longitudinal profile of $Bi_2O_3$ vaporization in sample A2[a]

| | XRF intensity (Kcps) | $[Bi_2O_3]$ from $IQ^+$ (wt.%)[b] | Calculated $[Bi_2O_3]$ (wt.%) | % $Bi_2O_3$ vaporized |
|---|---|---|---|---|
| External surface | 32092 | 1.78 | 1.73 | 31.7 |
| Slice 2 | 34012 | 1.82 | 1.84 | 27.6 |
| Slice 3 | 35728 | 2.04 | 1.93 | 24.0 |
| Slice 4 | 37536 | 2.12 | 2.03 | 20.1 |
| Slice 5 | 38340 | 2.02 | 2.07 | 18.4 |
| Compact center | 38519 | 2.00 | 2.08 | 18.0 |
| Green compact | 47008 | 2.55 | 2.54[c] | |

[a] *A*/*V* = 1.3 $cm^{-1}$.
[b] RSD ± 0.30, corresponding to $\sigma < 0.01\%$.
[c] Formulated composition.

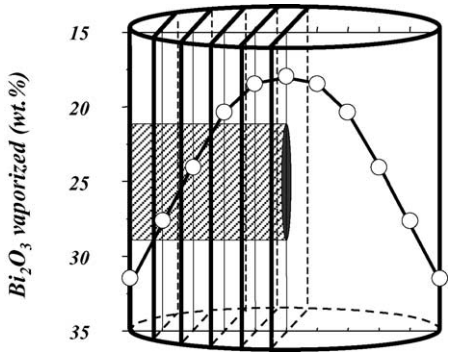


Fig. 2. Longitudinal gradient of $Bi_2O_3$ vaporization (in wt.%) for sample A2, from the external surface to the center of the varistor ceramic. *A*/*V* ratio = 1.3 $cm^{-1}$. Shaded zone corresponds to the XRF analyzed area (Ø = 27 mm).

Table 4
Transversal profile of $Bi_2O_3$ vaporization in sample A3[a]

| | XRF intensity (Kcps) | Calculated [$Bi_2O_3$] (wt.%) | % $Bi_2O_3$ vaporized |
|---|---|---|---|
| Upper slice | 8033 | 1.00 | 60.7 |
| Slice 2 | 8272 | 1.03 | 59.5 |
| Slice 3 | 8324 | 1.03 | 59.2 |
| Slice 4 | 8708 | 1.08 | 57.4 |
| Slice 5 | 8711 | 1.08 | 57.3 |
| Slice 6 | 8745 | 1.09 | 57.2 |
| Floor slice | 8991 | 1.12 | 56.0 |
| Green compact | 20425 | 2.54[b] | |

[a] *A*/*V* = 4.1 $cm^{-1}$.
[b] Formulated composition.

Finally, Fig. 4 shows the XRF intensities registered for sample A3 in the vicinity of the BiL$\alpha_1$ radiation. Together with the green sample and the upper and bottom external slices, it is also represented the spectrum corresponding to sample A4 prepared in the same conditions as A3 but without $Bi_2O_3$. As it can be seen, no interference from the other varistor constituents is affecting the intensity of this radiation line of Bi.

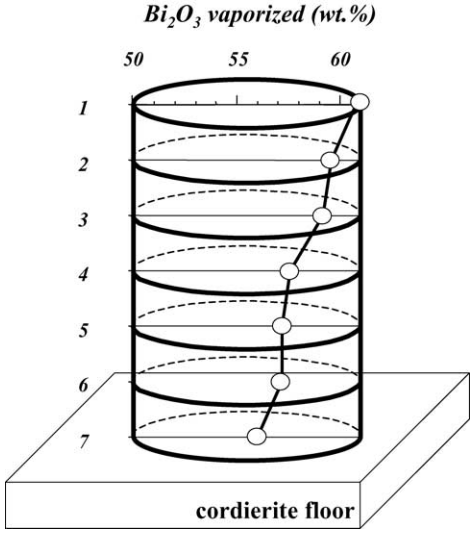


Fig. 3. Gradient of $Bi_2O_3$ vaporization in wt.% for a ceramic compact with higher *A*/*V* ratio: sample A3, *A*/*V* = 4.1 $cm^{-1}$. This time the whole area was analyzed by XRF (Ø < 27 mm).

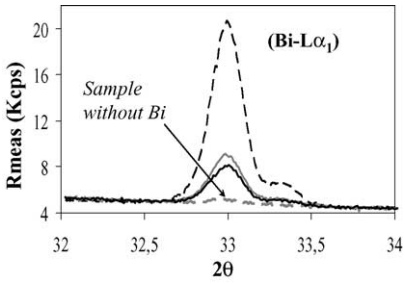


Fig. 4. XRF spectra for sample A3 in the vicinity of BiL$\alpha_1$ radiation. Black dashed line: green compact; grey line: bottoms slice; black bold line: upper slice.

## 4. Discussion

What is first inferred from results in previous section is that $Bi_2O_3$ vaporization is not homogeneous throughout the ceramic body. To keep equilibrium between the liquid phase and the reaction atmosphere, those areas nearby the surface have a lower content of $Bi_2O_3$ than the interior, with a longer way for $Bi_2O_3$ to leak out. However, this is not only a consequence of distance since, as densification proceeds during sintering, channels between ZnO grains become closed isolating the liquid at triple and multiple junctions which can only diffuse through the grain boundaries. As a result diffusion and vaporization from within the ceramic is more hindered than in the proximity of the surface. In this way, samples A1 and A2 have the highest $Bi_2O_3$ content in slices corresponding to the centre of the ceramic body, slice 4 in sample A1 and slice 6 in sample A2.

Different behaviour is found in sample A3 in which $Bi_2O_3$ volatilization is to 60% of the initial content, quite high compared to the maximum of 30% in samples A1 and A2. Moreover, in sample A3 vaporization decreases from the upper slice and the highest $Bi_2O_3$ content is not at the centre of the ceramic body but on the bottom of he specimen. The reason of this different behaviour is the total exposed area to the surface. The *A*/*V* ratio in sample A3 is 4.1 $cm^{-1}$ while in the other two samples it is only 1.3 $cm^{-1}$, which means that $Bi_2O_3$ has more surface to vaporize from sample A3. Similar behaviour is supposed to take place in all of the samples, but in A3 the diffusion paths to the outer atmosphere are shorter, resulting in small differences between the different slices (Table 4). In fact the lower vaporization of the bottom slice in sample A3 seems to be related to the physical presence of the varistor powder over the cordierite sheet. It is not significant in samples with lower *A*/*V* ratios.

All of these changes in composition from the $Bi_2O_3$ loss will obviously affect the microstructure of the sintered material. Since it has been found that vaporization is not homogenous along the ceramic body, the development of

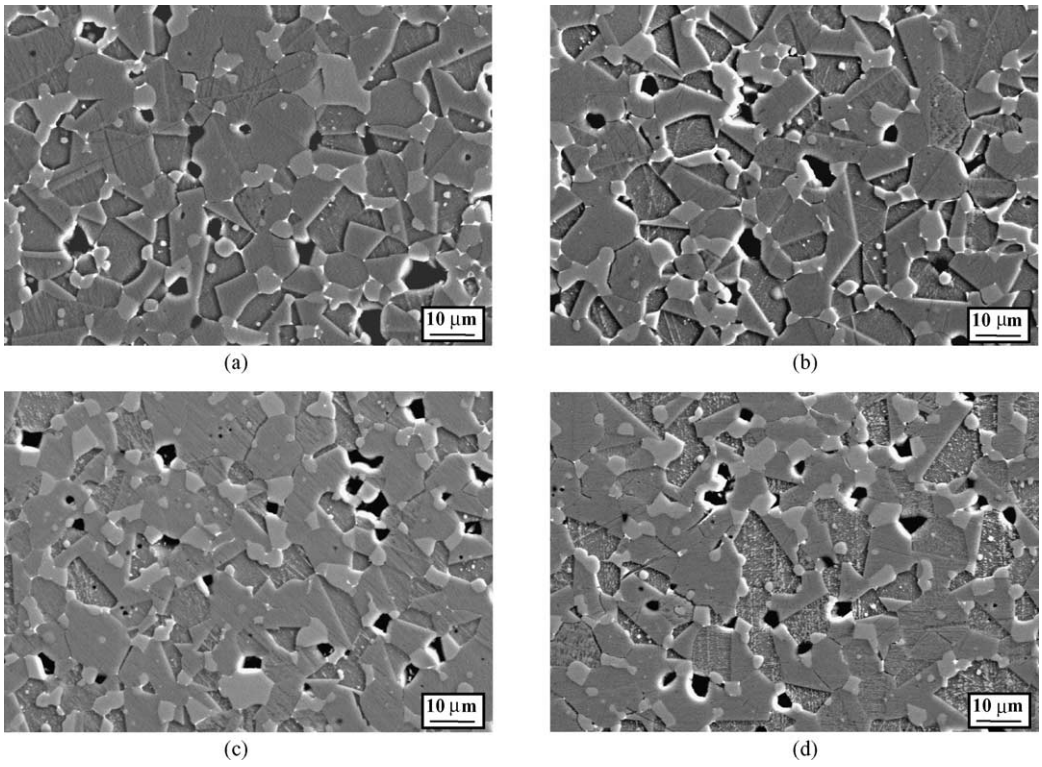


Fig. 5. SEM micrographs for different slices in sample A1 and A3. (a) Upper slice in sample A1, (b) middle slice in sample A1, (c) upper slice in sample A3 and (d) bottom slice in sample A3. *A*/*V* ratio equal to 1.3 and 4.1 $cm^{-1}$ for A1 and A3, respectively.

microstructure should also be expected to be different depending on the distance to the surface. A significant feature of the varistor microstructure is ZnO grain growth. The kinetics is strongly determined by the presence of the $Bi_2O_3$-rich liquid phase. Table 5 illustrates the results of grain size measurements for the slices of samples A1 and A3 with significant changes in $Bi_2O_3$ vaporization. From this table and the SEM micrographs in Fig. 5, it can be noted that the ZnO grain size increases with higher $Bi_2O_3$ contents that is with less $Bi_2O_3$ vaporization. Matter diffusion through the $Bi_2O_3$-rich liquid involve solution-precipitation processes (Ostwald-Rippening)[13] that are affected as the composition and total amount of liquid phase decreases. Vaporization of $Bi_2O_3$ modifies the nature of the Bi-rich liquid phase in such a way that the kinetics of these diffusion mechanisms becomes slower and ZnO grain growth is then reduced. Therefore, the more the $Bi_2O_3$-rich liquid phase vaporizes, the smaller the ZnO grain size. This is also reflected in the data from Table 5, in which we found a larger ZnO grain size in sample with lower *A*/*V* ratios that is with a higher $Bi_2O_3$ content.

On the other hand in sample A1 we find differences up to 16% in $Bi_2O_3$ losses between slices, which do not result in great differences in ZnO grain size, while in sample A3 small differences of only 4% are enough to see big changes in this microstructural parameter. This is more noticeable when plotting $Bi_2O_3$ vaporization versus ZnO grain size for both samples together, as depicted in Fig. 6. The shape of this curve indicates that grain size decreases with the amount of $Bi_2O_3$ vaporization. In this way, in sample A1 the loss of $Bi_2O_3$ reaches values of about 30% in the slice with higher

Table 5
Average ZnO grain size

| | % $Bi_2O_3$ vaporized | Grain size (±0.5 μm) |
|---|---|---|
| Slice 1 in A1[a] | 29.7 | 9.5 |
| Slice 5 in A1 | 13.8 | 10.1 |
| Slice 1 in A3[b] | 60.7 | 7.2 |
| Slice 7 in A3 | 56.0 | 8.6 |

[a] *A*/*V* ratio = 1.3 $cm^{-1}$.
[b] *A*/*V* ratio = 4.1 $cm^{-1}$.

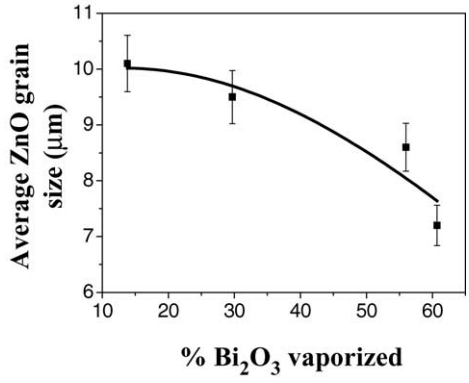


Fig. 6. Evolution of ZnO grain size as a function of $Bi_2O_3$ vaporization.

vaporization detected, so there remains a high content of bismuth oxide even in this slice, and no big differences in ZnO grain size could be observed. Vaporization in sample A3 however reaches values of 56% almost double that of sample A1, so that the $Bi_2O_3$ content is particularly low in all of its slices to create significant differences in the grain growth kinetics.

## 5. Conclusions

$Bi_2O_3$ vaporization in ZnO-based ceramic varistors was studied. It is observed to occur as a function of the distance to the surface area exposed to the sintering atmosphere. In this way the *A*/*V* ratio of the green ceramic plays a determining role in varistor manufacturing, since it limits the total amount of liquid Bi-rich phase that will be lost by vaporization. Microstructural development and more specifically the kinetics of ZnO grain growth are strongly affected by this vaporization in such a way that the grain size of ZnO tends to decrease with increasing bismuth oxide vaporization.

## Acknowledgements

The financial support of this research work by C001999 AX012 (CICYT) and MAT 2001-1682-C02-01 projects is gratefully acknowledged.

## References

1. Matsuoka, M., Nonohmic properties of zinc oxide ceramics. *Jpn. J. Appl. Phys.*, 1971, **10**(6), 736–746.
2. Eda, K., Conduction mechanism of nonohmic zinc oxide ceramics. *J. Appl. Phys.*, 1978, **49**(5), 2964–2972.
3. Clarke, D. R., Varistor ceramics. *J. Am. Ceram. Soc.*, 1999, **82**(3), 485–502.
4. Gupta, T. K., Applications of zinc oxide ceramics. *J. Am. Ceram. Soc.*, 1990, **73**(7), 1817–1840.
5. Look, D. C., Recent advances in ZnO materials and devices. *Mater. Sci. Eng.*, 2001, **80**, 383–387.
6. Inada, M., Formation mechanism of nonohmic zinc oxide ceramics. *Jpn. J. Appl. Phys.*, 1980, **19**(3), 409–419.
7. Olsson, E., Dunlop, G. L. and Österlund, R., Development of functional microstructure during sintering of a ZnO varistor material. *J. Am. Ceram. Soc.*, 1993, **76**(1), 61–75.
8. Morris, W. G., Electrical properties of ZnO–$Bi_2O_3$ ceramics. *J. Am. Ceram. Soc.*, 1973, **56**(7), 360–364.
9. Takemura, T., Kobayashi, M., Takada, Y. and Sato, K., Effects of bismuth sesquioxide on the characteristics of ZnO varistors. *J. Am. Ceram. Soc.*, 1986, **69**(5), 430–436.
10. Safronov, G. M., Batog, V. N., Stepanyuk, T. V. and Fedorov, P., Equilibrium diagram of the bismuth oxide-zinc oxide system. *Russ. J. Inorg. Chem.*, 1971, **16**(3), 460–461.
11. Dey, D. and Bradt, R. C., Grain growth of ZnO during $Bi_2O_3$ liquid-phase sintering. *J. Am. Ceram. Soc.*, 1992, **75**(9), 2529–2534.
12. Leite, E. R., Nobre, M. A. L., Longo, E. and Varela, J. A., Microstructural development of ZnO varistor during reactive liquid-phase sintering. *J. Mater. Sci.*, 1996, **31**, 5391–5398.
13. German, R. M., *Liquid Phase Sintering*. Plenum Press, New York, 1985.
14. Kim, J., Kimura, T. and Yamaguchi, T., Sintering of zinc oxide doped with antimony oxide and bismuth oxide. *J. Am. Ceram. Soc.*, 1989, **72**(8), 1390–1395.
15. Ott, J., Lorenz, A., Harrer, M., Preissner, E. A., Hesse, C., Feltz, A., Whitehead, A. H. and Schreiber, M., The influence of $Bi_2O_3$ and $Sb_2O_3$ on the electrical properties of ZnO-based varistors. *J. Electroceram.*, 2001, **6**(2), 135–146.
16. Olsson, E. and Dunlop, G. L., The effect of $Bi_2O_3$ content on the microstructure and electrical properties of ZnO varistor materials. *J. Appl. Phys.*, 1989, **66**(9), 4317–4324.
17. Magnusson, K. O. and Wiklund, S., Interface formation of Bi on ceramic ZnO: a simple model varistor grain boundary. *J. Appl. Phys.*, 1994, **76**(11), 7405–7409.
18. Greuter, F., Electrically active interfaces in ZnO varistors. *Solid State Ionics*, 1995, **75**, 67–78.
19. Wang, H. and Chiang, Y. M., Thermodynamic stability of intergranular amorphous films in bismuth-doped zinc oxide. *J. Am. Ceram. Soc.*, 1998, **81**(1), 89–96.
20. Metz, R., Machado, C., Elkhatib, M., Counioux, J. J., Delalu, H. and Al Abdullah, K., Stabilité thermique de composés intervenants au tours du frittage des varistances ZnO (thermal stability of components during sintering of ZnO varistors). *Sil. Ind.*, 2001, **66**(1-2), 15–22.
21. Wong, J., Sintering and varistor characteristics of ZnO–$Bi_2O_3$ ceramics. *J. Appl. Phys.*, 1980, **51**(8), 4453–4459.
22. Metz, R., Delalu, H., Vignalou, J. R., Achard, N. and Elkhatib, M., Electrical properties of varistors in relation to their true bismuth composition after sintering. *Mater. Chem. Phys.*, 2000, **63**, 157–162.
23. Caballero, A. C., Valle, F. J. and Martín Rubí, J. A., Determination of dopants in ZnO-based ceramic varistors by X-ray fluorescence and inductively coupled plasma spectrometry. *X-Ray Spectrom.*, 2001, **30**, 273–279.
24. Kim, J., Kimura, T. and Yamaguchi, T., Effect of bismuth oxide content on the sintering behavior of zinc oxide. *J. Am. Ceram. Soc.*, 1989, **72**(8), 1541–1544.
25. Senda, T. and Bradt, R. C., Grain growth in sintered ZnO and ZnO–$Bi_2O_3$ ceramics. *J. Am. Ceram. Soc.*, 1990, **73**(1), 106–114.
26. Chiang, Y-M., Kingery, W. D. and Levinson, L. M., Compositional changes adjacent to grain boundaries during electrical degradation of a ZnO varistor. *J. Appl. Phys.*, 1982, **53**(3), 1765–1768.
27. De la Rubia, M. A., Peiteado, M., Fernández, J. F. and Caballero, A. C., Compact shape as a relevant parameter for sintering ZnO–$Bi_2O_3$ based varistors. *J. Eur. Ceram. Soc.*, 2004, **24**(6), 1209–1212.